A&A 536, A51 (2011)
DOI: 10.1051/0004-6361/201117348

Astronomy & Astrophysics

Atomic data of Zn I for the investigation of element abundances*

Y. P. Liu[1], C. Gao[1], J. L. Zeng[1], and J. R. Shi[2]

[1] Department of Physics, College of Science, National University of Defense Technology, 410073 Changsha, Hunan, PR China
e-mail: jiaolongzeng@hotmail.com
[2] National Astronomical Observatories, Chinese Academy of Sciences, 100012 Beijing, PR China

Received 26 May 2011 / Accepted 9 September 2011

ABSTRACT

Aims. We calculate the energy levels, oscillator strengths, and photoionization cross-sections of Zn I to provide atomic data for the study of element abundances in astrophysics.
Methods. The calculations are carried out by using the R-matrix method in the LS-coupling scheme. The lowest 12 terms of Zn II are utilized as target states and extensive configuration interaction is included to properly delineate the quantum states of Zn II and Zn I.
Results. The 3443 oscillator-strength values are calculated in both length and velocity forms, for the dipole-allowed transitions between 235 bound states of Zn I. The photoionization cross-section of each bound state is presented in a photon energy range from the first threshold to about 1.5 Ry. Some resonance structures are identified in the photoionization cross-sections.
Conclusions. A set of atomic data to derive the spectral characteristics of neutral zinc is obtained. Comparisons are made with available experimental and other theoretical results.

Key words. stars: abundances – atomic data

1. Introduction

Accurate determination of the abundance of zinc is important to investigate the chemical evolution of both damped Lyα systems (Pettini et al. 1997) and our Galaxy (Allen et al. 2011; Bihain et al. 2004). Bisterzo et al. (2004) determined the Zn abundances for stars of different stellar populations and metallicities based on high resolution spectra. Using the most widely available stellar nucleosynthesis expectations, they found that the abundance of zinc is central to inferring its astrophysical origin. It has been recognized that it is important to consider the effects of non-local thermodynamic equilibrium (NLTE) when determining element abundances (Asplund 2005). Research has shown that NLTE can strongly affect the abundances of Na, Mg, Al, Si, K, and Ca (Andrievsky et al. 2007, 2008, 2010; Gehren et al. 2004, 2006; Mashonkina et al. 2008; Shi et al. 2008) and these effects are sensitive to the accuracy of the atomic data used in the NLTE modeling. An adequate atomic model requires a complete set of atomic data, and the development of such a model is a difficult task for Zn owing to its complex atomic structure (Mishenina et al. 2002). To the best of our knowledge, the only published study of the effects of NLTE of Zn abundance is Takeda et al. (2005), who used the photoionization cross-sections derived from hydrogenic approximation. There is therefore an urgent need to obtain a complete set of accurate atomic data for Zn.

Energy levels, oscillator strengths, and photoionization cross-sections are the basic atomic parameters. The energy levels of Zn I were published by Moore (1971) and comprehensively summarized by Sugar & Musgrove (1995), whereas the oscillator strengths and the photoionization cross-sections of Zn I are not widely available in the literature.

Experimental studies of the oscillator strengths of Zn I were addressed by Landman & Novick (1964) and Lurio et al. (1964), who measured the lifetime of the excited state $3d^{10}4s4p\ ^1P^\circ$. The lifetimes of more quantum states including $3d^{10}4s4p\ ^1P^\circ$ were measured by Martinson et al. (1979) and Zerne et al. (1994). Kerkhoff et al. (1980) measured the oscillator strengths for transitions of $3d^{10}4sns\ ^3S$–$3d^{10}4smp\ ^3P^\circ$ and $3d^{10}4sn'd\ ^3D$–$3d^{10}4smp\ ^3P^\circ$ ($n = 5$–$7, n' = 4$–$6, m = 4, 5$). From the theoretical point of view, Hibbert (1989) calculated the oscillator strength of the resonance transition $3d^{10}4s^2\ ^1S$–$3d^{10}4s4p\ ^1P^\circ$ using model potentials. The oscillator strength of the same transition was discussed by Brage & Froese Fischer (1992) using a multi-configuration Hartree-Fock (MCHF) approach that considered the core polarization effects. Glowacki & Migdalek (2006) and Chen & Cheng (2010) carried out relativistic configuration interaction (CI) calculations for the transition rates of $3d^{10}4s^2\ ^1S_0$–$3d^{10}4s4p\ ^1P^\circ_1$ and $3d^{10}4s^2\ ^1S_0$–$3d^{10}4s4p\ ^3P^\circ_1$.

Most investigations of the photoionization of Zn I have focused on the ground state $3d^{10}4s^2\ ^1S$. Marr & Austin (1969) and Harrison et al. (1969) measured the photoionization cross-section of Zn I in the photon energy range of 0.69–1.22 and 0.73–3.69 Ry, respectively. The *d*-shell absorption spectrum was presented and analyzed by Sommer et al. (1987) using synchrotron radiation as the background source. Photoionization cross-sections for the 4s, 3d, 3p, 3s subshells of Zn I were calculated by Fliflet & Kelly (1974, 1976) using many-body perturbation theory. Bartschat (1987) calculated the photoionization cross-section of the ground state $3d^{10}4s^2\ ^1S$ for Zn I by using the semirelativistic R-matrix method based on the Breit-Pauli Hamiltonian, while Stener & Decleva (1997) presented time-dependent local density approximation (TDLDA) calculations

* The complete set of atomic data is only available at the CDS via anonymous ftp to cdsarc.u-strasbg.fr (130.79.128.5) or via http://cdsarc.u-strasbg.fr/viz-bin/qcat?J/A+A/536/A51

for the photoionization of the ground state. Froese Fischer & Zatsarinny (2007) calculated the photoionization of the 4s4p excited states using the MCHF approach and the B-spline R-matrix method.

The atomic data presented above, either experimental or theoretical, are insufficient for building a practical NLTE model for the investigation of the Zn abundance, as such a model would need a complete and consistent set of atomic data involving a large number of quantum states. In this work, we aim to provide a complete set of atomic data including the energy levels, oscillator strengths, and photoionization cross-sections for Zn I. The present calculations are carried out using the R-matrix program[1], which is a modified version of the Belfast atomic R-matrix program RMATRX1 (Berrington et al. 1995). Extensive CI is taken into account to ensure that accurate atomic data can be obtained.

2. Theoretical methods

The R-matrix method is a kind of close-coupling approach to the analysis of electron-atom and photon-atom interactions, which was described in great detail by Burke et al. (1971) and Berrington et al. (1987). The outline of this method is briefly presented in the following, where LS-coupling is assumed. In the internal region, the wave functions of the $(N + 1)$-electron system are depicted as linear combinations of the energy-independent basis states ψ_k that are expanded in the form

$$\psi_k(X_1...X_{N+1}) = \hat{A}\sum_{ij} c_{ijk}\Phi_i(X_1...X_N\hat{r}_{N+1}\sigma_{N+1})u_{ij}(r_{N+1}) + \sum_j d_{jk}\phi_j(X_1...X_{N+1}), \quad (1)$$

where $\hat{A}$ is the antisymmetrization operator that takes the exchange effects between the target electrons and the $(N + 1)$th electron into account, and i is the channel symbol. The term X_m stands for the spatial ($\boldsymbol{r}_m$) and the spin (σ_m) coordinates of the mth electron. The Φ_i are channel functions consisting of CI wavefunctions for the residual ion coupled with spin-angle functions for the $(N+1)$th electron to give an eigenstate of definite total orbital angular momentum L and total spin S. The functions $u_{ij}(r)$ in the first term on the right hand side of Eq. (1), which are normally obtained from appropriate equations and boundary conditions, form the basis sets for the continuum wavefunctions of the $(N + 1)$th electron. The $\{\phi_j\}$ in the second term on the right hand side of Eq. (1) are $(N + 1)$-electron bound states that are eigenstates with the same L and S, and they are included to allow for electron correlation effects. In the external region, the exchange effects between the target electrons and the $(N + 1)$th electron have been ignored and the radial functions $F_i(r)$ of the $(N + 1)$th electron can be obtained by directly integrating the radial equations. Matching the two regions at the R-matrix radius provides a scattering matrix and the wave functions of the $(N+1)$-electron system, hence the dipole transition probabilities.

The one-electron orbitals of bound states from which the $\{\phi_j\}$ are constructed are represented as linear combinations of Slater-type orbitals

$$P_{nl}(r) = \sum_j C_{jnl} r^{I_{jnl}} \exp(-\zeta_{jnl} r), \quad n > l, \quad (2)$$

where the parameters C_{jnl} and ζ_{jnl} are determined variationally by optimizing the energies of specific LS-coupled states. In practice, the Slater-type coefficients C_{jnl} are replaced by Clementi-type coefficients G_{jnl} as

$$C_{jnl} = G_{jnl}\frac{(2\zeta_{jnl})^{I_{jnl}+\frac{1}{2}}}{\sqrt{(2I_{jnl})!}}. \quad (3)$$

In this work, we employed 12 orbitals of Zn II. The orbitals 1s, 2s, 2p, 3s, 3p, 3d, 4s were chosen to be HF functions given by Clementi & Roetti (1974) for the ground state $3d^{10}4s\ ^2S$ of Zn II. However, 3d and 4s were adjusted by minimizing a linear combination of the ground state and $3d^94s^2\ ^2D$ with the CIV3 computer code (Hibbert 1975). The orbitals 4p, 4d, 5s, 5p were obtained by optimizing linear combinations of the energies of the corresponding $3d^{10}n$l (occupying a weight of 99.6%) and $3d^94sn'l'$ (the same LS term as $3d^{10}n$l occupying a weight of 0.4%) states, respectively. The only pseudo orbital $\overline{5d}$ was obtained by optimizing the state of $3d^94s^2\ ^2D$. The relevant parameters of the valence orbital radial functions are listed in Table 1.

The R-matrix radius was chosen to be 36.0 a.u. to ensure that the wavefunctions of bound states were completely wrapped within the R-matrix sphere. As for the construction of the continuum states, the number of the continuum basis functions $u_{ij}(r)$ was set to be 75. The 12 lowest terms of Zn II were utilized as target states, whose energy levels are listed in Table 2.

To adequately describe the target states, extensive CI was included in the present work. To show the CI effects on the energy levels of the target states, we present three sets of calculations in Table 2, which are represented by cases A, B, and C, respectively. In case A, a single electron excitation is allowed from 3d and 4s subshells of the ground configuration $3d^{10}4s$ excluding $\overline{5d}$ subshell. Explicitly, configurations of $3d^{10}4s$, $3d^{10}4p$, $3d^{10}4d$, $3d^{10}5s$, $3d^{10}5p$, $3d^94s^2$, $3d^94s4p$, $3d^94s4d$, $3d^94s5s$, and $3d^94s5p$ were included in the calculation. In case B, in addition to configurations included in case A, two electron excitations are allowed from 3d and 4s subshells of the configuration $3d^94s^2$, excluding $\overline{5d}$ subshell. Therefore, in addition to configurations included in case A, the following configurations were taken into account: $3d^94p^2$, $3d^94p4d$, $3d^94p5s$, $3d^94p5p$, $3d^94d^2$, $3d^94d5s$, $3d^94d5p$, $3d^95s^2$, $3d^95s5p$, $3d^95p^2$, $3d^84s^24p$, $3d^84s^24d$, $3d^84s^25s$, $3d^84s^25p$, $3d^84s4p^2$, $3d^84s4p4d$, $3d^84s4p5s$, $3d^84s4p5p$, $3d^84s4d^2$, $3d^84s4d5s$, $3d^84s4d5p$, $3d^84s5s^2$, $3d^84s5s5p$, $3d^84s5p^2$, $3d^74s^24p^2$, $3d^74s^24p4d$, $3d^74s^24p5s$, $3d^74s^24p5p$, $3d^74s^24d^2$, $3d^74s^24d5s$, $3d^74s^24d5p$, $3d^74s^25s^2$, $3d^74s^25s5p$, and $3d^74s^25p^2$. In case C, two electron excitations are allowed from either the 3d or 4s subshells of the configuration $3d^94s^2$, including excitations to the $\overline{5d}$ subshell, and five additional configurations are included to describe the target states. In addition to the configurations included in cases A and B, the following configurations were included in case C: $3d^{10}5d$, $3d^94s5d$, $3d^94p5d$, $3d^94d5d$, $3d^95s5d$, $3d^95p5d$, $3d^95d^2$, $3d^84s^25d$, $3d^84s4p5d$, $3d^84s4d5d$, $3d^84s5s5d$, $3d^84s5p5d$, $3d^84s5d^2$, $3d^84p^25d$, $3d^84p4d5d$, $3d^84p5s5d$, $3d^84p5p5d$, $3d^84p5d^2$, $3d^74s^24p5d$, $3d^74s^24d5d$, $3d^74s^25s5d$, $3d^74s^25p5d$, and $3d^74s^25d^2$.

In Table 2, we also give the experimental energy levels compiled by Sugar & Musgrove (1995). One can find that the energies of the target states become closer and closer to the experimental results as the CI scale increases from case A to C. In the following, all results on the energy levels, oscillator strengths, and photoionization cross-sections were obtained by using the CI in case C.

[1] http://amdpp.phys.strath.ac.uk/tamoc/code.html

Table 1. Orbital parameters of the radial functions obtained with the CIV3 code for Zn II.

Orbital	I_{jnl}	ζ_{jnl}	G_{jnl}
4s	1	29.37180	−0.02755
	1	43.90184	−0.00078
	2	24.30800	−0.02481
	2	13.41410	0.11150
	3	11.61883	0.05541
	3	6.94016	−0.04771
	3	5.70187	−0.27299
	4	5.35544	0.01710
	4	1.56435	0.12925
	4	2.30879	0.52431
	4	1.43454	0.42013
5s	1	29.41116	−0.01337
	1	39.99134	−0.00017
	2	24.47343	−0.00771
	2	13.41635	0.04387
	3	13.11934	0.01398
	3	9.48467	−0.00585
	4	7.51909	−0.11466
	4	1.90753	0.33874
	5	2.92789	0.10153
	5	0.89896	−1.03800
4p	2	11.94328	0.09343
	2	12.59519	−0.18468
	3	1.71598	−0.65911
	3	5.50624	0.27239
	4	3.33035	0.12626
	4	1.27619	−0.51414
5p	2	11.81203	−0.01322
	2	22.30131	−0.00087
	3	9.04742	−0.00174
	3	6.68251	0.02664
	4	6.23318	0.01046
	4	2.94166	−0.02826
	5	1.35556	−0.33933
	5	0.65840	1.12143
3d	3	4.99622	0.40869
	3	15.05086	0.01740
	3	8.13694	0.22736
	3	3.01409	0.36344
	3	1.89919	0.14661
4d	3	4.51050	0.34752
	3	12.98563	0.00697
	3	8.07623	0.00155
	4	5.70563	−0.19306
	4	1.38234	−0.33363
	4	0.81239	−0.72891
$\overline{5d}$	3	6.80623	−0.10585
	3	5.55932	0.80360
	4	14.69261	−0.01318
	4	7.02005	−0.43908
	5	1.94243	−0.84904
	5	0.73561	0.81200

3. Results and discussions

Using the method described above, we calculated the energy levels of the bound states, bound-bound oscillator strengths, and photoionization cross-sections of Zn I.

3.1. Bound states of Zn I

We obtained 235 bound states of different symmetries (characterized by total orbital angular momentum and spin and parity) in this work. The energy levels of some of the lowest bound states and several high Rydberg states are listed in Table 3, together with the experimental data (Sugar & Musgrove 1995). From the inspection of Table 2, one can see that the calculated energies of the target states are a little lower than the experimental results, except for the term of $3d^9 4s^2\ ^2D$. This shows that the energy of the ground term $3d^{10}4s\ ^2S$ was slightly overestimated in the calculation. Such an overestimate is due to the complexity of atomic structure of Zn. To better describe $3d^{10}4s\ ^2S$ and $3d^9 4s^2\ ^2D$, one has to include electron correlations with three and four electron excitations from orbital 3d and higher orbitals, such as that of $n = 6$. Nevertheless such a larger scale of CI is untractable. In addition, relativistic effects may play a role in describing atomic structure. As a result, the energy of the ground term $3d^{10}4s^2\ ^1S$ of Zn I was overestimated. The calculated ionization energy of Zn I is 0.66614 Ry. To make a more helpful comparison with the experiment, we set the energy of the ground term $3d^{10}4s^2\ ^1S$ of Zn I to 0.02432 Ry in Table 3, which is the difference between the calculated and experimental value (0.69046 Ry). In this way, most of the calculated energy levels are in closer agreement with the experimental data.

Table 2. Energy levels (in Ry) for the target states of Zn II in different scales of configuration interaction.

Target states	A	B	C	Expt.
$3d^{10}4s\ ^2S$	0.00000	0.00000	0.00000	0.00000
$3d^{10}4p\ ^2P^\circ$	0.42674	0.43755	0.43814	0.44710
$3d^9 4s^2\ ^2D$	0.72210	0.63651	0.61746	0.58148
$3d^{10}5s\ ^2S$	0.72675	0.73776	0.79578	0.80590
$3d^{10}4d\ ^2D$	0.81105	0.82349	0.86067	0.88338
$3d^{10}5p\ ^2P^\circ$	0.84985	0.86583	0.92440	0.92521
$3d^9 4s4p(^3P^\circ)\ ^4P^\circ$	1.00426	0.96445	0.94100	0.95422
$3d^9 4s4p(^3P^\circ)\ ^4F^\circ$	1.02850	0.98918	0.96595	0.97608
$3d^9 4s4p(^3P^\circ)\ ^4D^\circ$	1.07043	1.02887	1.00121	1.01626
$3d^9 4s4p(^3P^\circ)\ ^2F^\circ$	1.07209	1.03317	1.01102	1.01757
$3d^9 4s4p(^3P^\circ)\ ^2P^\circ$	1.09739	1.05334	1.02187	1.03426
$3d^9 4s4p(^3P^\circ)\ ^2D^\circ$	1.09853	1.05719	1.03080	1.04357

Notes. Experimental data are given for comparison.

Several high Rydberg states given in Table 3 show the correct order of energy even at the principal quantum numbers $n = 18$, 19, and 20. For the states with high principal quantum number n, the energies tend to be degenerate. For example, the energies of $3d^{10}4s8g\ ^3G$ (0.67481 Ry), $3d^{10}4s8h\ ^3H^\circ$ (0.67483 Ry), and $3d^{10}4s8i\ ^3I$ (0.67484 Ry) are very close and nearly degenerate. Such a conclusion is consistent with the basic theory of atomic structure and spectra (Cowan 1981). The treatment of this degeneracy of Rydberg states is a great challenge of the theory. One must be very careful to assign the correct state order in the calculations. The energies of a Rydberg series become closer to the experimental values as the principal quantum number n increases, which can be found from $3d^{10}4snp\ ^1P^\circ$ and $3d^{10}4snd\ ^1D$ ($n = 8, 10, 14, 18–20$) of the Rydberg series. This indicates that our method is effective for high Rydberg states.

3.2. Oscillator strengths

For the zinc atom, the observed lines are mainly concentrated into bound-bound transitions between configurations of the Rydberg series $3d^{10}4snl$ ($n = 4–7$, $l = 0, 1, 2$) (Ralchenko et al. 2010). In Table 4, we compare our calculated weighted oscillator strengths (gf-values) for some dipole allowed transitions with experimental and other theoretical results in the literature.

Table 3. Energy levels (in Ry) of bound states for Zn I.

Bound states	This work	Experiment
$3d^{10}4s^2\ {}^1S$	0.02432	0.0
$3d^{10}4s4p\ {}^3P^\circ$	0.28778	0.29795
$3d^{10}4s4p\ {}^1P^\circ$	0.43341	0.42598
$3d^{10}4s5s\ {}^3S$	0.49271	0.48910
$3d^{10}4s5s\ {}^1S$	0.51111	0.50839
$3d^{10}4s5p\ {}^3P^\circ$	0.55800	0.55863
$3d^{10}4s4d\ {}^1D$	0.56474	0.56915
$3d^{10}4s4d\ {}^3D$	0.56999	0.57204
$3d^{10}4s5p\ {}^1P^\circ$	0.57427	0.57328
$3d^{10}4s6s\ {}^3S$	0.59777	0.59626
$3d^{10}4s6s\ {}^1S$	0.60302	0.60178
$3d^{10}4s6p\ {}^3P^\circ$	0.62066	0.62049
$3d^{10}4s5d\ {}^1D$	0.62075	0.62275
$3d^{10}4s5d\ {}^3D$	0.62459	0.62496
$3d^{10}4s6p\ {}^1P^\circ$	0.62568	0.62520
$3d^{10}4s4f\ {}^3F^\circ$	0.62718	0.62726
$3d^{10}4s4f\ {}^1F^\circ$	0.62718	0.62726
$3d^{10}4s7s\ {}^3S$	0.63625	0.63557
$3d^{10}4s7s\ {}^1S$	0.63853	0.63792
$3d^{10}4s7p\ {}^3P^\circ$	0.64700	0.64688
$3d^{10}4s6d\ {}^1D$	0.64626	0.64746
$3d^{10}4s6d\ {}^3D$	0.64878	0.64894
$3d^{10}4s7p\ {}^1P^\circ$	0.64924	0.64900
$3d^{10}4s5f\ {}^3F^\circ$	0.65001	0.65006
$3d^{10}4s5f\ {}^1F^\circ$	0.65001	0.65006
$3d^{10}4s5g\ {}^3G$	0.65036	0.65041
$3d^{10}4s8s\ {}^1S$	0.65605	0.65571
$3d^{10}4s8p\ {}^3P^\circ$	0.66076	0.66068
$3d^{10}4s7d\ {}^1D$	0.66006	0.66082
$3d^{10}4s8p\ {}^1P^\circ$	0.66196	0.66182
$3d^{10}4s6f\ {}^3F^\circ$	0.66241	0.66241
$3d^{10}4s6g\ {}^3G$	0.66262	0.66258
$3d^{10}4s6h\ {}^3H^\circ$	0.66267	0.66278
$3d^{10}4s8d\ {}^1D$	0.66832	0.66883
$3d^{10}4s7f\ {}^3F^\circ$	0.66987	0.66978
$3d^{10}4s7g\ {}^3G$	0.67001	0.66994
$3d^{10}4s7h\ {}^3H^\circ$	0.67004	0.67010
$3d^{10}4s7i\ {}^3I$	0.67005	0.67028
$3d^{10}4s10p\ {}^1P^\circ$	0.67452	0.67446
$3d^{10}4s8g\ {}^3G$	0.67481	0.67471
$3d^{10}4s8h\ {}^3H^\circ$	0.67483	0.67483
$3d^{10}4s8i\ {}^3I$	0.67484	0.67494
$3d^{10}4s10d\ {}^1D$	0.67726	0.67751
$3d^{10}4s14p\ {}^1P^\circ$	0.68342	0.68340
$3d^{10}4s14d\ {}^1D$	0.68425	0.68434
$3d^{10}4s18p\ {}^1P^\circ$	0.68652	0.68651
$3d^{10}4s18d\ {}^1D$	0.68687	0.68691
$3d^{10}4s19p\ {}^1P^\circ$	0.68697	0.68696
$3d^{10}4s19d\ {}^1D$	0.68726	0.68730
$3d^{10}4s20p\ {}^1P^\circ$	0.68735	0.68734
$3d^{10}4s20d\ {}^1D$	0.68760	0.68763
ZnII(^{2}S)Limit	0.69046	0.69046

The on-line data provided by Kurucz[2] are also listed, which were mostly derived from the theoretical work of Warner (1968), in only a few of cases from experiments. Experimental values are given between the fine-structure levels instead of LS-coupled terms, hence we give the gf-values according to LS terms wherever possible. The symbol "*" denotes that the experimental data do not contain any contribution to the final states of $J_f = 1$, as a result the experimental data are smaller in value than our theoretical results. Most gf-values in length form in Table 4 have a relative difference of smaller than 20% with experimental data. For the transition of 4s4p ^{1}P°–4s6s ^{1}S, the relative difference between gf-values in length form of this work and that of Warner is 50%. For this transition, the oscillator strength is very small and thus sensitive to the wavefunctions and CI included in the calculation. Warner carried out his calculation based on the scaled Thomas-Fermi-Dirac (STFD) wavefunctions, which differs from those adopted in the present work.

As an illustrative example, we give the weighted oscillator strengths of transitions between the Rydberg series of $3d^{10}4snd\ {}^3D$ and $3d^{10}4sn'f\ {}^3F^\circ$ of Zn I in Table 5. Some gf-values in Table 5 are negative, because the initial and final terms are reversed. Taking transition series 4s4d−4snf, 4s5d − 4smf, 4s4f−4snd and 4s5f−4smd (n = 4−12, m = 5−12) as examples, one can find that as the principal quantum number n increases, the oscillator strengths of a Rydberg series generally decrease quite fast. This can be understood qualitatively from the general trends of oscillator strengths (Cowan 1981). For a Rydberg series of transition, among other factors such as transition energies and angular momentum, the oscillator strengths and the effective quantum numbers n^* have the approximate relation

$$gf(n_i l_i \gamma_i J_i M_i - n_f l_f \gamma_f J_f) \propto (n_j^*)^{-3}, \quad (4)$$

and this relation stands reasonably for higher principal quantum number n_j.

From the inspection of Tables 4 and 5, generally good agreements are found between the length and velocity forms of our oscillator strengths. In Table 5, the relative differences between the length and velocity forms are smaller than 7%. In Table 4, such a relative difference is smaller than 30% (majority of which are smaller than 10%) except for transitions of ^{1}S–^{1}P°. For the transitions of 4s^2 ^{1}S–4s4p ^{1}P° and 4s4p ^{1}P°–4s5s ^{1}S, the length form of oscillator strengths agree better with the experiments, hence the length form is more reliable. To evaluate the quality of the calculated oscillator strengths as a whole, we show the velocity form versus the length form of absolute gf-values in Fig. 1 for the bound-bound transitions whose absolute gf-values are greater than 0.001 in all of the 3443 dipole-allowed transitions. Since the data cover five orders of magnitude, we adopted the logarithm coordinates for both the length and velocity forms. For thousands of calculated gf-values, nearly all of them are centered at the line corresponding to equality between the two forms, especially for larger gf-values. Such a generally good agreement between the velocity and length forms of the oscillator strengths is an indication of quality for the present calculation, although scope remains for some improvement in the accuracy of the results.

3.3. Photoionization cross-sections

In stellar atmospheres, photoionization of neutral species are crucial because they are photoionization-dominated atoms (Asplund 2005). Photoionization cross-sections are much more important for the ground and several lowest excited states. In the following, we present in detail the photoionization cross-sections of the ground state $3d^{10}4s^2\ {}^1S$, the first excited state $3d^{10}4s4p\ {}^3P^\circ$, the second excited state $3d^{10}4s4p\ {}^1P^\circ$, and the third excited state $3d^{10}4s5s\ {}^3S$ for Zn I, although the photoionization cross-sections of all bound states were performed in a photon energy range from the first threshold to about 1.5 Ry in this work. Furthermore, the Rydberg series of $3d^{10}4sns$ (n = 5−8) ^{3}S are presented to show the general trend of a Rydberg series.

[2] http://kurucz.harvard.edu/linelists.html

Table 4. gf-values compared with experimental data and other theoretical results for Zn I.

Transitions	Length	Velocity	Experiments	Other calculations
$4s^2\ ^1S$–$4s4p\ ^1P^\circ$	1.514	0.836	1.49[a] , 1.46[b] , 1.55[c] , 1.449[d]	1.526[g] , 1.493[h] , 1.48[i] , 1.559[j] , 1.608[k]
$4s5p\ ^1P^\circ$	0.096	0.027		0.122[d]
$4s4p\ ^1P^\circ$–$4s5s\ ^1S$	0.466	0.295	0.501[d] , 0.444[e]	
$4s6s\ ^1S$	0.016	0.008		0.024[d]
$4s4d\ ^1D$	1.289	1.335	1.44[e]	1.413[d] ,1.338[h]
$4s4p\ ^3P^\circ$–$4s5s\ ^3S$	1.201	1.373	1.27[f]	1.342[d]
$4s6s\ ^3S$	0.146	0.185	0.145[f]	0.131[d]
$4s7s\ ^3S$	0.051	0.062	0.054[f]	0.046[d]
$4s4d\ ^3D$	4.084	3.404	3.687[d] , 4.12[e] , 3.89[f]	
$4s5d\ ^3D$	1.058	0.858	1.064[d] , 1.071[f]	
$4s6d\ ^3D$	0.445	0.355	*0.346[f]	
$4s5s\ ^1S$–$4s5p\ ^1P^\circ$	1.219	1.100		1.349[d]
$4s5s\ ^3S$–$4s5p\ ^3P^\circ$	3.874	4.054		3.947[d]
$4s5p\ ^3P^\circ$–$4s6s\ ^3S$	2.492	2.474	2.77[f]	2.487[d]
$4s7s\ ^3S$	0.211	0.220	0.155[f]	0.181[d]
$4s5d\ ^3D$	3.219	3.015	4.02[f]	
$4s6d\ ^3D$	0.971	0.902	*0.85[f]	

References. [(a)] Landman & Novick (1964); [(b)] Lurio et al. (1964); [(c)] Martinson et al. (1979); [(d)] http://kurucz.harvard.edu/linelists.html; [(e)] Ralchenko et al. (2010); [(f)] Kerkhoff et al. (1980); [(g)] Chen & Cheng (2010); [(h)] Froese Fischer & Zatsarinny (2007); [(i)] Glowacki & Migdalek (2006); [(j)] Brage & Froese Fischer (1992); [(k)] Hibbert (1989).
Notes. "*" Without contribution from states of $J_f = 1$.

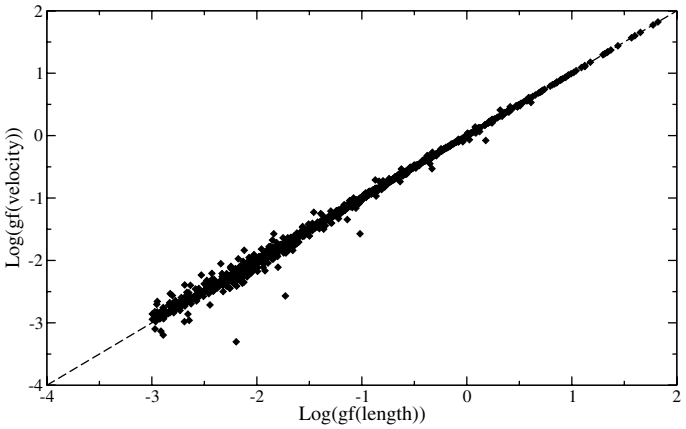

Fig. 1. Velocity vs. length forms for the oscillator strengths of Zn I.

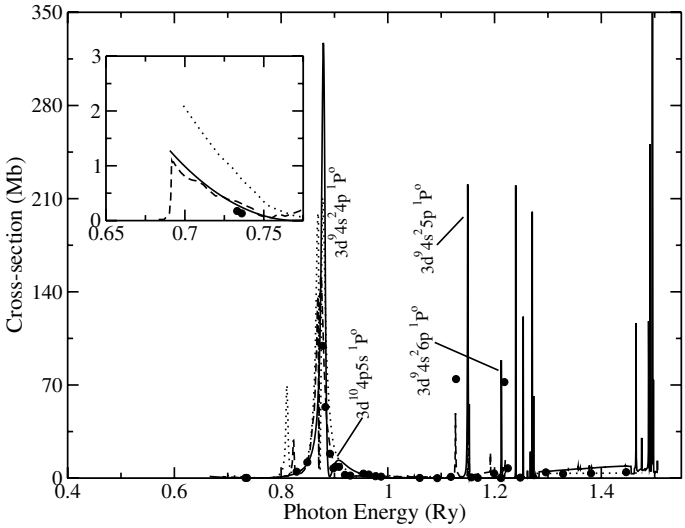

Fig. 2. Photoionization cross-section for the ground state $3d^{10}4s^2\ ^1S$ of Zn I. The solid line represents the cross-section in the present work. The dotted line represents the theoretical result carried out by Bartschat (1987). The dashed line and the filled circles represent the experimental data from Marr & Austin (1969) and Harrison (1969), respectively. The inset at the top left corner is the cross-section near threshold shown on an expanded scale.

Figure 2 shows the photoionization cross-section for the ground state of Zn I in a solid line. To compare with the experimental results, we show the experimental data from Marr & Austin (1969) and Harrison et al. (1969) as a dashed line and filled circles, respectively. The cross-section near the threshold is shown on an expanded scale at the top left corner, and is shifted by 0.02432 Ry, which is the difference between the calculated ionization potential of the ground state and the experimental value shown in Table 3. In the energy range of the $3d^94s^24p$ resonance, Marr & Austin's experiment exhibited three resonance peaks, a weak resonance at about 0.82 Ry of the photon energy and the double maximum near 0.87 Ry. The authors labeled the weak resonance at 0.82 Ry as $3d^94s^24p\ ^1P^\circ_1$, and the double maximum as resonances $3d^94s^24p\ ^3P^\circ_1$ and $3d^94s^24p\ ^3D^\circ_1$. Nevertheless, there is clearly inconsistency among the energy levels of Zn I (Sugar & Musgrove 1995), because the energy levels of $3d^94s^24p\ ^3P^\circ_1$, $3d^94s^24p\ ^3D^\circ_1$, and $3d^94s^24p\ ^1P^\circ_1$ are 0.82221, 0.86761, and 0.87292 Ry, respectively. Moreover, the transition probability of the dipole allowed transition $3d^{10}4s^2\ ^1S_0$–$3d^94s^24p\ ^1P^\circ_1$ should be stronger than the dipole forbidden transitions $3d^{10}4s^2\ ^1S_0$–$3d^94s^24p\ ^3P^\circ_1$ and $3d^{10}4s^2\ ^1S_0$–$3d^94s^24p\ ^3D^\circ_1$. Fortunately, Bartschat (1987) analyzed these resonances with a semirelativistic R-matrix method, which enabled them to classify the weak resonance at 0.82 Ry as $3d^94s^24p\ ^3P^\circ_1$, and to establish that the double maximum near 0.87 Ry originated from the interference of the strong $3d^94s^24p\ ^1P^\circ_1$ resonance with the weak $3d^94s^24p\ ^3D^\circ_1$ resonance that in turn produced a minimum located in the center of the strong $3d^94s^24p\ ^1P^\circ_1$ resonance peak. The photoionization cross-section obtained by Bartschat is indicated by a dotted line in Fig. 2. The resonances of $3d^94s^25p\ ^1P^\circ_1$, $3d^94s^26p\ ^1P^\circ_1$, and

Table 5. gf-values for the transition series $3d^{10}4snd\ ^3D$–$3d^{10}4sn'f\ ^3F^\circ$ of Zn I.

Initial	Final	Length	Velocity	Rel. diff.
4s4d	4s4f	13.330	12.800	4.0%
	4s5f	2.5150	2.3800	5.4%
	4s6f	0.9209	0.8657	6.0%
	4s7f	0.4495	0.4210	6.3%
	4s8f	0.2569	0.2401	6.5%
	4s9f	0.1623	0.1515	6.7%
	4s10f	0.1098	0.1024	6.7%
	4s11f	0.0781	0.0728	6.8%
	4s12f	0.0577	0.0538	6.8%
4s5d	4s4f	1.9990	1.9460	2.7%
	4s5f	10.440	10.290	1.4%
	4s6f	2.6310	2.5850	1.7%
	4s7f	1.0950	1.0740	1.9%
	4s8f	0.5747	0.5629	2.1%
	4s9f	0.3446	0.3373	2.1%
	4s10f	0.2253	0.2204	2.2%
	4s11f	0.1565	0.1530	2.2%
	4s12f	0.1136	0.1111	2.2%
4s6d	4s4f	−0.4324	−0.4547	5.2%
	4s5f	3.3430	3.3760	1.0%
	4s6f	9.3130	9.3780	0.7%
	4s7f	2.5990	2.6180	0.7%
	4s8f	1.1450	1.1490	0.3%
	4s9f	0.6237	0.6229	0.1%
	4s10f	0.3841	0.3819	0.6%
	4s11f	0.2563	0.2539	0.9%
	4s12f	0.1809	0.1787	1.2%
4s7d	4s4f	−0.0708	−0.0736	4.0%
	4s5f	−1.0340	−1.0560	2.1%
4s8d	4s4f	−0.0249	−0.0255	2.4%
	4s5f	−0.1806	−0.1870	3.5%
4s9d	4s4f	−0.0119	−0.0121	1.7%
	4s5f	−0.0652	−0.0680	4.3%
4s10d	4s4f	−0.0068	−0.0068	0.0%
	4s5f	−0.0318	−0.0333	4.7%
4s11d	4s4f	−0.0043	−0.0043	0.0%
	4s5f	−0.0183	−0.0191	4.4%
4s12d	4s4f	−0.0029	−0.0029	0.0%
	4s5f	−0.0116	−0.0122	5.2%

$3d^94s^24f\ ^1P^\circ_1$ are not shown as the maximal cross-sections of these resonances were unknown from Fig. 1 given by Bartschat. Since the LS-coupling scheme is used in this work, the present approach cannot reproduce the spin forbidden transitions from the ground term $3d^{10}4s^2\ ^1S$ to $3d^94s^24p\ ^3P^\circ$ and $3d^94s^24p\ ^3D^\circ$ autoionization states.

For the photoionization of the first excited state $3d^{10}4s4p\ ^3P^\circ$ of Zn I, there are three allowed final channels ^3S, ^3P and ^3D according to the dipole selection rule. The partial waves ^3S and ^3D contain a contribution from the first ionization threshold 0.40268 Ry, while the energetically lowest ionization channel of partial wave ^3P opens from the second ionization threshold $3d^{10}4p\ ^2P^\circ$ (0.84082 Ry). Figure 3 shows these partial-wave cross-sections and the total cross-section of $3d^{10}4s4p\ ^3P^\circ$, where the partial-wave cross-sections of ^3S, ^3P, and ^3D are displayed in the sub-pictures (a), (b), and (c) respectively, and the total cross-section is displayed in (d). Solid lines in Fig. 3 represent the length forms of the cross-sections, while dashed lines represent the velocity form, and the two forms closely agree with each other. It can be seen that the ^3P partial cross-section clearly contains a contribution from the photon energy of 0.9 Ry. In Figs. 3a and 3c, the first autoionization resonances of partial waves ^3S and ^3D are produced by the configuration $3d^{10}4p5p$, not by the configuration $3d^{10}4p^2$, because two equivalent electrons in the 4p subshell cannot form the triplet symmetries ^3D and ^3S according to the Pauli exclusion principle. Figure 3c also shows a broad and strong resonance, which should be caused by $3d^94s4p^2\ ^3D$, whose positions are in the energy range of the resonances $3d^94s^2nd\ ^3D$ ($n = 4, 5$). These resonances of the partial ^3D are much stronger than any other partial symmetries ^3S and ^3P in the shown photon energy range.

Figures 4a and 4b show the partial photoionization cross-sections of ^1S and ^1D for the second excited state $3d^{10}4s4p\ ^1P^\circ$ of Zn I. As the first excited triplet state $3d^{10}4s4p\ ^3P^\circ$, the ^1S and ^1D partial-wave photoionization cross-sections for the second excited state contain a contribution from the first ionization threshold 0.25705 Ry, while the energetically lowest ionization channel of the partial wave ^1P opens from the second ionization threshold $3d^{10}4p\ ^2P^\circ$ (0.69519 Ry) and its partial cross-section is lower than 0.01 Mb until the photon energy exceeds 0.86 Ry. Therefore, we did not give the partial cross-section of ^1P symmetry. Solid and dashed lines represent the length and velocity forms of photoionization cross-sections, respectively. It is quite clear that the first resonances of ^1D and ^1S partial waves for the photoionization cross-sections of $3d^{10}4s4p\ ^1P^\circ$ are both produced by the configuration $3d^{10}4p^2$.

From the inspection of Fig. 4, it can be seen that the autoionization resonances of $3d^{10}4p^2\ ^1S$ and ^1D have completely different characteristics. The former is narrow with an autoionization width being about 0.004 Ry and the peak cross-section of nearly 300 Mb, while the latter is a giant resonance with a width exceeding 0.1 Ry. To distinguish more clearly the resonance of $3d^{10}4p^2\ ^1S$, the cross-section near the resonance are redrawn in the inset of Fig. 4a on a logarithmic scale. These two resonances were carefully investigated by Froese Fischer & Zatsarinny (2007) using both the MCHF and B-spine R-matrix methods and their results are shown in Fig. 4 in dotted lines. To enable a clearer comparison, their results have been shifted by 0.007 Ry toward lower photon energy. One can see that there is generally good agreement between our own and their results near the two resonances.

Photoionization cross-sections of the Rydberg series $3d^{10}4sns\ ^3S$ ($n = 5$, 6, 7, and 8) are displayed in Fig. 5. One can see that with the increase in the principal quantum number n, the ionization potential decreases, and the cross-section in the threshold increases, but it falls off fast as photon energy increases near the threshold. This is consistent with the basic theory of atomic structure (Cowan 1981). For photoionization of the Rydberg state with a high principal quantum number n, the cross-section near the threshold tends to be hydrogenic according to

$$\sigma \sim n\left(\frac{\varepsilon_n}{\varepsilon_p}\right)^3, \tag{5}$$

where ε_n is the threshold ionization energy for the shell n, and ε_p is the photon energy. In addition, the peak value of the same resonance decreases from the top down for $3d^94s^24p$, $3d^{10}4p5s$, and $3d^94s^25p\ ^3P^\circ$ autoionization states, yet for higher n autoionized states such as $3d^{10}4pns$ and $3d^{10}4pnd\ ^3P^\circ$, the strongest photoionization cross-section occurs for the respective state of $3d^{10}4sns\ ^3S$, where the principal quantum number n is identical to that of the autoionized states. This conclusion is similar to the bound-bound transitions, as shown in Table 5, which considers the transitions of $3d^{10}4snd\ ^3D$–$3d^{10}4sn'f\ ^3F^\circ$ of Zn I as an example to illustrate such characteristics. For transitions from the state of $4s4d\ ^3D$, the value of the oscillator strengths decreases

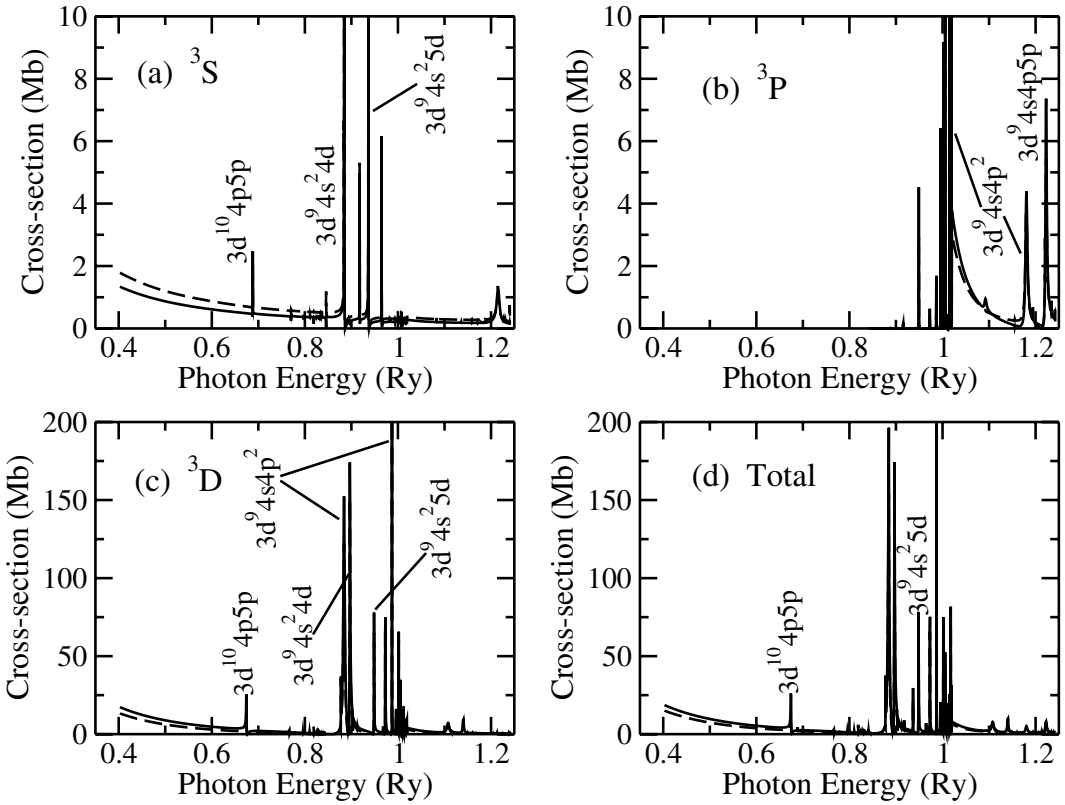

Fig. 3. Photoionization cross-sections for the first excited state $3d^{10}4s4p\ ^3P^\circ$ of Zn I. The partial wave cross-sections of ^{3}S, ^{3}P and ^{3}D are displayed in **a)**, **b)**, and **c)**, respectively, and the total cross-section is displayed in **d)**. The solid lines represent the length forms of cross-sections, and the dashed lines represent velocity forms.

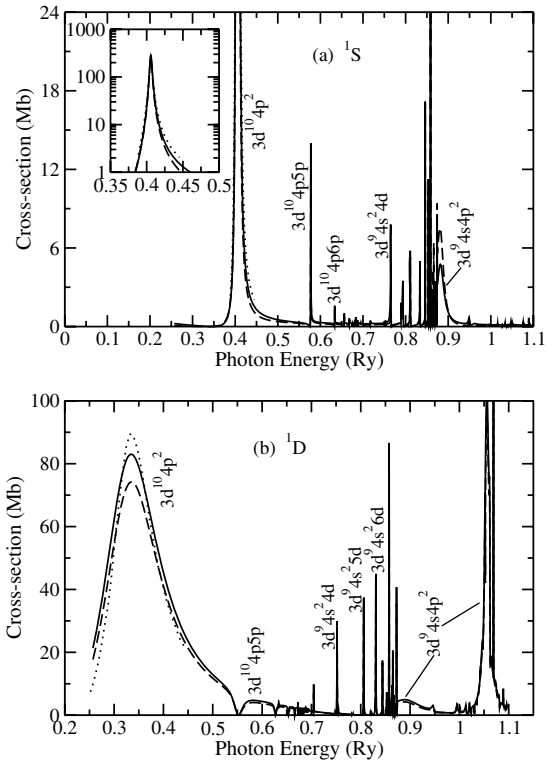

Fig. 4. ^{1}S and ^{1}D partial photoionization cross-sections of $3d^{10}4s4p\ ^1P^\circ$ for Zn I. Solid and dashed lines represent the length and velocity forms of cross-sections, and the dotted lines represent the theoretical results carried out by Froese Fischer & Zatsarinny (2007). The inset in **a)** is the cross-section near the resonance of $3d^{10}4p^2\ ^1$S on a logarithmic scale.

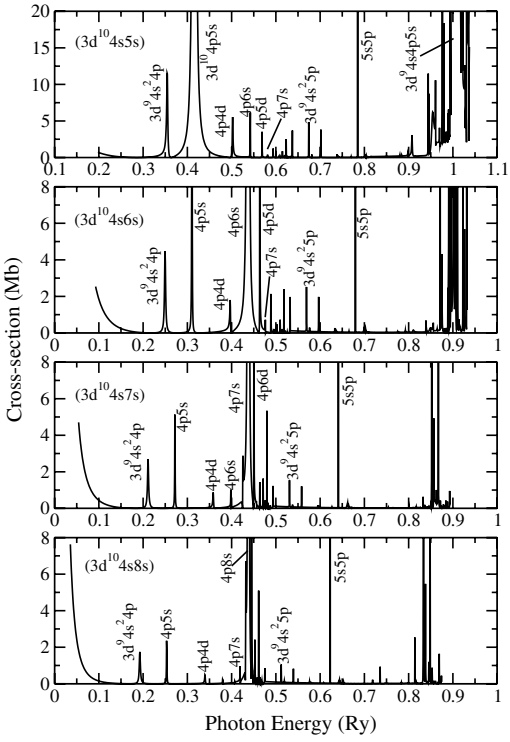

Fig. 5. Photoionization cross-sections of the Rydberg series $3d^{10}4sns\ ^3$S (n = 5–8 from the top down).

with increasing Rydberg series of $3d^{10}4sn'f\ ^3F^\circ$, while for transitions from the initial state of $4s5d\ ^3D$, the maximal oscillator strengths occurs for $3d^{10}4s5f\ ^3F^\circ$, not for $3d^{10}4s4f\ ^3F^\circ$.

Some autoionization resonances are identified and labeled in Figs. 2–5 and the resonance positions are listed in Table 6. The energically lowest autoionized state corresponds to $3d^{10}4p^2\ ^1D$ and the second lowest to $3d^{10}4p^2\ ^1S$. As discussed in the above, $3d^{10}4p^2\ ^1D$ is a giant resonance with the autoionizing width exceeding 0.1 Ry. This giant resonance will surely play an important role in the NLTE modeling of element abundance determination not only owing to its large photoionization cross-section, but also to its low photon energy.

In conclusion, a complete set of atomic data including the energies of bound states, oscillator strengths of electric dipole transitions between these bound states, and the photoionization cross-sections of all bound states of Zn I were obtained by a close-coupling approach implemented using the R-matrix method. The complete set of atomic data are available upon request and at the CDS. To achieve a clearer representation of the target and $N+1$ electronic states, we included adequate electron correlations in the calculation. Detailed comparisons are made with available experimental and theoretical results in the literature. For the oscillator strengths and photoionization cross-sections, generally good agreement is found between the length and velocity forms. Some resonances shown in the photoionization cross-sections are identified. The energically lowest autoionized state $3d^{10}4p^2\ ^1D$ and the second lowest one $3d^{10}4p^2\ ^1S$ may play an important role in the NLTE modeling of element abundance determination. The former one is a giant resonance with autoionizing width exceeding 0.1 Ry and the latter contains strong absorption of the incident radiation.

Acknowledgements. This work was supported by the National Natural Science Foundation of China under Grants Nos. 10878024, 10774191, and 10734140, and the National Basic Research Program of China (973 Program) under Grant No. 2007CB815105.

Table 6. Energy levels of autoionization states for Zn I obtained from analyzing the resonance structures shown in photoionization cross-sections (Figs. 2–5).

States	Terms	Levels(Ry)
Zn II limit	^2S	0.69046
$3d^{10}4p^2$	^1D	0.768
	^1S	0.839
$3d^{10}4p5s$	$^3P^\circ$	0.908
	$^1P^\circ$	0.932
$3d^{10}4p5p$	^3D	0.962
	^3S	0.976
	^1D	1.003
	^1S	1.011
$3d^{10}4p4d$	$^3P^\circ$	0.995
	$^1P^\circ$	1.012
$3d^{10}4p6s$	$^3P^\circ$	1.035
	$^1P^\circ$	1.040
$3d^{10}4p6p$	^3D	1.054
	^3S	1.058
	^1D	1.067
	^1S	1.067
$3d^{10}4p5d$	$^3P^\circ$	1.061
	$^1P^\circ$	1.066
$3d^{10}4p7s$	$^3P^\circ$	1.074
	$^1P^\circ$	1.077
$3d^{10}4p7p$	^3D	1.083
	^3S	1.086
	^1D	1.089
	^1S	1.090
$3d^9 4s^2 4p$	$^3P^\circ$	0.847
	$^1P^\circ$	0.904
$3d^9 4s^2 5s$	^3D	1.104
$3d^9 4s^2 5p$	$^3P^\circ$	1.167
	$^1P^\circ$	1.174
$3d^9 4s^2 4d$	^3S	1.172
	^3D	1.185
	^1D	1.185
	^1S	1.199
$3d^9 4s^2 5d$	^3S	1.224
	^3D	1.236
	^1D	1.237
$3d^{10}5s5p$	$^3P^\circ$	1.282
$3d^9 4s4p^2$	^3D	1.172
	^3D	1.275
	^3P	1.305
	^3P	1.468
	^1D	1.489
$3d^9 4s4p5s$	$^3P^\circ$	1.504
$3d^9 4s4p5p$	^3P	1.510

References

Allen, D. M., & Porto, de Mello, G. F. 2011, A&A, 525, A63
Andrievsky, S. M., Spite, M., Korotin, S. A., et al. 2007, A&A, 464, 1081
Andrievsky, S. M., Spite, M., Korotin, S. A., et al. 2008, A&A, 481, 481
Andrievsky, S. M., Spite, M., Korotin, S. A., et al. 2010, A&A, 509, A88
Asplund, M. 2005, ARA&A, 43,481
Bartschat, K. 1987, J. Phys. B, 20, 5023
Berrington, K. A., Burke, P. G., Butler, K., et al. 1987, J. Phys. B, 20, 6379
Berrington, K. A., Eissner, B. W., & Norrington, P. H. 1995, Comput. Phys. Commun., 92, 290
Bihain, G., Israelian, G., Rebolo, R., et al. 2004, A&A, 423, 777
Bisterzo, S., Gallino, R., Pignatari, M., et al. 2004, Mem. S. A. It., 75, 741
Brage, T., & Froese Fischer, C. 1992, Phys. Scr., 45, 43
Burke, P. G., Hibbert, A., & Robb, W. D. 1971, J. Phys. B, 4, 153
Chen, M. H., & Cheng, K. T. 2010, J. Phys. B, 43, 074019
Clementi, E., & Roetti, C., 1974, At. Data Nucl. Data Tables, 14, 177
Cowan, R. D. 1981, The theory of atomic structure and spectra (Berkeley: University of California Press)
Fliflet, A. W., & Kelly, H. P. 1974, Phys. Rev. A, 10, 508
Fliflet, A. W., & Kelly, H. P. 1976, Phys. Rev. A, 13, 312
Froese Fischer, C., & Zatsarinny, O. 2007, Theor. Chem. Account, 118, 623
Gehren, T., Liang, Y. C., Shi, J. R., et al. 2004, A&A, 413, 1045
Gehren, T., Shi, J. R., Zhang, H. W., et al. 2006, A&A, 451, 1065
Glowacki, L., & Migdalek, J. 2006, J. Phys. B, 39, 1721
Harrison, H., Shoen, R. I., & Cairns, R. B. 1969, J. Chem. Phys., 50, 3930
Hibbert, A. 1975, Comput. Phys. Commun., 9, 141
Hibbert, A. 1989, Phys. Scr., 39, 574
Kerkhoff, H., Schmidt, M., & Zimmermann, P. 1980, Z. Phys. A, 298, 249
Landman, A., & Novick, R. 1964, Phys. Rev., 134, A56
Lurio, A., de Zafra, R. L., & Goshen, R. J. 1964, Phys. Rev., 134, A1198
Marr, G. V., & Austin, J. M. 1969, J. Phys. B, 2, 107
Martinson, I., Curtis, L. J., Huldt, S., et al. 1979, Phys. Scr., 19, 17
Mashonkina, L., Zhao, G., Gehren, T., et al. 2008, A&A, 478, 529
Mishenina, T. V., Kovtyukh, V. V., Soubiran, C., et al. 2002, A&A, 396, 189
Moore, C. E. 1971, Atomic Energy Levels 2. Natl. Stand. Ref. Data. Ser., Natl. Bur. Stand. (US), 35 (Washington DC: US GPO)
Pettini, M., Smith, L. J., King, D. L., et al. 1997, ApJ, 486, 665
Ralchenko, Yu., Kramida, A. E., Reader, J., et al. 2010, NIST Atomic Spectra Database (Ver. 4.0.0), http://physics.nist.gov/asd, National Institute of Standards and Technology, Gaithersburg, MD
Shi, J. R., Gehren, T., Butler, K., et al. 2008, A&A 486, 303
Sommer, K., Baig, M. A., & Hormes, J. 1987, Z. Phys. D, 4, 313
Stener, M., & Decleva, P. 1997, J. Phys. B, 30, 4481
Sugar, J., & Musgrove, A. 1995, J. Phys. Chem. Ref. Data, 24, 1803
Takeda, Y., Hashimoto, O., Taguchi, H., et al. 2005, PASJ, 57, 751
Warner, B. 1968, MNRAS, 140, 53
Zerne, R., Luo, C. Y., Jiang, Z. K., et al. 1994, Z. Phys. D, 32, 187